

Bulk and surface electronic structure of hexagonal WC

L. F. Mattheiss and D. R. Hamann

AT&T Bell Laboratories, Murray Hill, New Jersey 07974

(Received 15 March 1984)

The bulk and surface electronic structure of hexagonal WC have been investigated by means of self-consistent scalar relativistic calculations that apply the linear augmented-plane-wave method. The surface studies consider WC(0001)-W(1×1) and -C(1×1) faces and assume a slab geometry with bulk interlayer spacings. Separate calculations have been carried out for symmetrical nine-layer slabs containing either W(1×1) or C(1×1) surfaces and an asymmetrical eight-layer slab containing both. The bulk calculations show that WC is a semimetal with a low density of states (DOS) at E_F and a Fermi surface consisting of several small electron and hole pockets. According to the surface studies, both the W(1×1) and C(1×1) faces exhibit distinctive surface-state features and an enhanced surface DOS near E_F . The calculated work function for the W surface, $\phi(W)=5.2$ eV, is 1.2 eV smaller than that for C. Additional differences between the two surfaces are reflected in the corrugation amplitudes of the charge density in the vacuum region. These features will be useful for establishing the surface composition in experimental studies on WC(0001) samples.

I. INTRODUCTION

The monocarbides of transition elements from the group-IVB, -VB, and -VIB columns of the Periodic Table are well known for their great hardness and strength, high melting temperatures, metal-like thermal and electrical resistivities, nonstoichiometry, and superconducting properties.¹ Most experimental and theoretical efforts to understand the fundamental properties of these technologically important materials have focused thus far on the group-IVB and -VB carbides, all of which crystallize with the cubic rocksalt structure. Despite their structural simplicity, progress towards a comprehensive understanding of these materials has been inhibited by their nonstoichiometry and tendency to incorporate appreciable vacancy concentrations on both the metal and carbon sublattices.¹

Considerably less work has been done thus far on the group-VIB monocarbides. Chromium and molybdenum carbide are unstable at room temperature and are formed only by quenching from high temperatures. Tungsten carbide is stable at room temperature and crystallizes with a hexagonal rather than a cubic structure. This hexagonal WC compound is unique among the transition-metal-carbide family in yet another respect. Namely, high-quality single-crystal WC samples can be prepared with few vacancies and the ideal 1:1 stoichiometric composition. As a result, good WC single-crystal samples are found to exhibit lower electrical resistivities² [$\rho(4.2$ K) ≈ 0.5 vs $10 \mu\Omega$ cm] and larger residual resistance ratios^{2,3} [$\rho(300$ K)/ $\rho(4.2$ K) ≈ 70 vs 2] than typical transition-metal carbides. This has permitted, for example, the recent observation of de Haas-van Alphen oscillations in this material,³ thereby providing the first detailed measurements of the WC Fermi surface.

In addition to its bulk properties, comparable interest in the surface electronic structure of WC has been generated by its promise as a catalytic agent. This has been particu-

larly true since the work of Levy and Boudart,⁴ who showed that WC exhibits catalytic properties which are similar to those of Pt but are totally unlike those of W. This led them to conclude that "the surface electronic properties of the latter are therefore modified by the carbon in such a way that they resemble those of platinum."

Bennett *et al.*⁵ have proposed that this WC-Pt similarity is not confined to the surface electronic structure, but extends to that of the bulk as well. By comparing valence-band x-ray photoemission spectroscopy (XPS) data for W, WC, and Pt, they have argued (neglecting transition probabilities) that the bulk WC density of states near E_F , $N(E_F)$, is intermediate between the corresponding W and Pt curves, where $N(E_F)$ falls near local minima and maxima, respectively. One problem with this proposal is that it conflicts with the relative values for the measured electronic specific-heat coefficients γ for W (Ref. 6) and WC (Ref. 1) for which $\gamma(W) > \gamma(WC)$.

In order to provide a better understanding of the bulk and surface electronic structure of hexagonal WC and to stimulate further experimental studies on this material, self-consistent, scalar relativistic energy-band calculations have been carried for WC in bulk and thin-film forms with the use of the linear augmented-plane-wave (LAPW) method.⁷ The surface studies have considered WC(0001) faces for which preliminary photoemission data have been reported.⁸ The surface calculations utilize an ideal (0001) slab geometry which involves alternate W and C hexagonal layers and bulk interlayer separations. Surface LAPW calculations have been carried out for symmetric nine-layer WC(0001) slabs with undistorted W(1×1) and C(1×1) faces and an asymmetric eight-layer slab which contains both.

The present bulk energy-band results for hexagonal WC are qualitatively similar to those obtained in previous studies,^{8,9} though differences are found in the band ordering near E_F .⁹ The stability of the hexagonal phase for the group-VIB carbides is reflected in the valence-band

density-of-states curve. This exhibits a minimum near E_F which falls close to the middle of a broad (~ 15 eV) $2p$ - $5d$ bonding-antibonding complex. The Fermi surface is that of a semimetal, consisting of several small electron and hole pockets whose dimensions are consistent with the de Haas-van Alphen data.³

The surface electronic structure calculations for the WC(0001)-W(1×1) and -C(1×1) faces predict several surface-state branches within the energy range $E_F \pm 2$ eV on both faces and, relative to the bulk, an increase in the surface density of states near E_F . The calculations further predict a 1.2-eV difference between the W(1×1) and C(1×1) work functions and a stronger corrugation of the vacuum charge density for the C(1×1) surface. These characteristics will be useful for identifying the surface-layer composition in experimental studies on WC(0001) samples.

The organization of this paper is as follows. The essential details of the present LAPW calculations are summarized in Sec. II, including an analysis of the hexagonal WC structure and its symmetry. The principal results of this investigation are presented and discussed in Sec. III. These include bulk and slab energy bands, density-of-states curves, and charge-density results.

II. COMPUTATIONAL DETAILS

A. WC structure

The hexagonal WC structure has the symmetry of the D_{3h}^1 ($P6m2$) space group. The structure contains a single WC formula unit per primitive cell. It consists of alternating simple-hexagonal layers of W and C atoms whose registry and rotational alignment is such that the nearest-neighbor coordination at both the W and C sites is trigonal prismatic. (See Fig. 1.) This is in contrast to the NaCl structure (which is characteristic of the group-IVB and -VB monocarbides) where the coordination at each site is octahedral. An intermediate structure is that of NiAs, where the nearest-neighbor coordination at a Ni site is octahedral while the corresponding As sites are surrounded by trigonal prisms of Ni atoms.

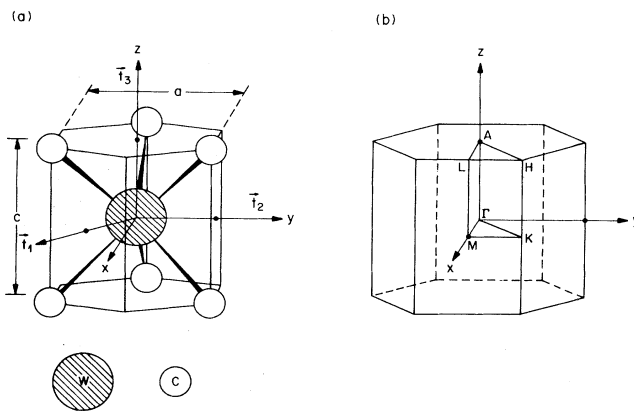


FIG. 1. Primitive unit cell (a) and Brillouin zone (b) for the hexagonal WC structure.

The primitive vectors that generate the hexagonal lattice can be written in the form

$$\vec{t}_1 = (a/2)(\sqrt{3}\hat{i} - \hat{j}), \quad \vec{t}_2 = a\hat{j}, \quad \vec{t}_3 = c\hat{k}, \quad (1)$$

where the lattice parameters a and c for WC are $a = 2.9065$ Å and $c = 2.8366$ Å, respectively.¹ In terms of this nonorthogonal coordinate system, the W and C atom positions are (0,0,0) and $(\frac{1}{3}, \frac{2}{3}, \frac{1}{2})$, respectively. The primitive unit cell for the hexagonal WC structure is shown in Fig. 1. The point symmetry at both the W and C sites is D_{3h} .

The primitive reciprocal-lattice vectors corresponding to Eq. (1) are given by

$$\vec{b}_1 = (4\pi/\sqrt{3}a)\hat{i}, \quad \vec{b}_2 = (2\pi/\sqrt{3}a)(\hat{i} + \sqrt{3}\hat{j}), \\ \vec{b}_3 = (2\pi/c)\hat{k}. \quad (2)$$

By means of the usual construction, these generate the familiar hexagonal Brillouin zone which is shown to the right in Fig. 1. It is noted that while the D_{3h} point group contains only half of the full-hexagonal (D_{6h}) symmetry operations, time-reversal symmetry¹⁰ causes the restoration of full-hexagonal symmetry to $E(\vec{k})$ and produces an irreducible Brillouin-zone (IBZ) wedge with $\frac{1}{24}$ rather than $\frac{1}{12}$ of the Brillouin-zone volume. This IBZ wedge is indicated by the solid lines in Fig. 1. Its vertices are labeled using standard notation.¹¹

In designating crystal directions and planes, the standard notation involving four indices is adopted. These directions and planes are written $[hkil]$ and $(hkil)$, respectively, with the condition $i = -(h+k)$. In terms of this notation, the ΓM , ΓK , and ΓA directions in Fig. 1 are $[10\bar{1}0]$, $[11\bar{2}0]$, and $[0001]$, respectively. Similarly, the ΓALM , $MLHK$, ΓAHK , and ΓMK planes are denoted by $(\bar{1}2\bar{1}0)$, $(\bar{1}100)$, $(10\bar{1}0)$, and (0001) , respectively.

Luehrmann¹¹ has worked out and tabulated the irreducible representations for all of the symmorphic space groups, including those for D_{3h}^1 . For convenience, his results and notation have been adopted in the present analysis and discussion of the WC structure. Group-theoretical methods can provide valuable information regarding the crystal wave-function composition at atomic sites for wave vectors \vec{k} at symmetry points in the Brillouin zone. In particular, using standard techniques, one can determine which angular-momentum states Y_{lm} can occur in a wave function that transforms according to a given irreducible representation of the D_{3h}^1 space group. The results of such an analysis for hexagonal WC are summarized in Table I. These results are sufficient for identifying the symmetry of energy-band states in calculational schemes like the present one where the basis functions are unsymmetrized.

The full D_{3h}^1 space-group symmetry of bulk WC is preserved for symmetric WC(0001) slabs that contain an odd number of layers. However, translational symmetry is now confined to the plane of the slab. This yields a two-dimensional surface Brillouin zone (SBZ) with an irreducible triangle $\bar{\Gamma} \bar{M} \bar{K}$ which is identical in size, shape, and symmetry with the ΓMK portion of the bulk BZ in Fig. 1.

TABLE I. Orbital-symmetry analysis at the W and C sites for the hexagonal WC structure (D_{3h}^1 space group).

	Γ	M	K	A	L	H
	W(0,0,0)					
s	1 ⁺	1	1	1 ⁺	1	1
p_z	2 ⁻	4	4	2 ⁻	4	4
p_x, p_y	3 ⁺	1,3	2,3	3 ⁺	1,3	2,3
$d_{3z^2-r^2}$	1 ⁺	1	1	1 ⁺	1	1
$d_{xy}, d_{x^2-y^2}$	3 ⁺	1,3	2,3	3 ⁺	1,3	2,3
d_{xz}, d_{yz}	3 ⁻	2,4	5,6	3 ⁻	2,4	5,6
	$C \left(\frac{1}{3}, \frac{2}{3}, \frac{1}{2} \right)$					
s	1 ⁺	1	3	2 ⁻	4	6
p_z	2 ⁻	4	6	1 ⁺	1	3
p_x, p_y	3 ⁺	1,3	1,2	3 ⁻	2,4	4,5

One can extend the methods used to generate the results in Table I to this (0001) slab geometry. We summarize briefly the results of this analysis at $\bar{\Gamma}$. For example, in the case of a central W-atom layer, the symmetry of s , p , and d states at $\bar{k}_{||} = \bar{0}$ ($s \rightarrow \bar{\Gamma}_{1+}; p \rightarrow \bar{\Gamma}_{2-}, \bar{\Gamma}_{3+}; d \rightarrow \bar{\Gamma}_{1+}, \bar{\Gamma}_{3+}, \bar{\Gamma}_{3-}$) is identical to that for the bulk (Table I). Noncentral W layers contribute additional states, often having different symmetry ($s \rightarrow \bar{\Gamma}_{2-}; p \rightarrow \bar{\Gamma}_{1+}, \bar{\Gamma}_{3-}; d \rightarrow \bar{\Gamma}_{2-}, \bar{\Gamma}_{3+}, \bar{\Gamma}_{3-}$). Similarly, for noncentral C-atom layers, the bulk-type states ($s \rightarrow \bar{\Gamma}_{1+}; p \rightarrow \bar{\Gamma}_{2-}, \bar{\Gamma}_{3+}; d \rightarrow \bar{\Gamma}_{1+}, \bar{\Gamma}_{3+}, \bar{\Gamma}_{3-}$) are supplemented by an equal number of extra states ($s \rightarrow \bar{\Gamma}_{2-}; p \rightarrow \bar{\Gamma}_{1+}, \bar{\Gamma}_{3-}; d \rightarrow \bar{\Gamma}_{2-}, \bar{\Gamma}_{3+}, \bar{\Gamma}_{3-}$) in a slab geometry where the size of the primitive cell is proportional to the number of layers in the slab.

The space-group symmetry is reduced from D_{3h}^1 to C_{3v}^1 ($P3m1$) for asymmetric slabs which contain an even number of layers. Because of the lost reflection symmetry, the surface states no longer occur in pairs such that sums and differences of nearly-degenerate slab state pairs [involving, for example, the symmetric slab combinations ($\bar{\Gamma}_{1+}, \bar{\Gamma}_{2-}$), ($\bar{\Gamma}_{2+}, \bar{\Gamma}_{1-}$), ($\bar{\Gamma}_{3+}, \bar{\Gamma}_{3-}$), etc.] yield wave functions which are localized on one surface or the other. Instead, individual surface states are already localized on the appropriate surface.

B. LAPW calculations

The present LAPW calculations have been carried out for both bulk and thin-film forms of WC. The latter calculations have involved related studies on three separate thin films. These include two symmetric nine-layer WC(0001) slabs with unrelaxed W(1×1) and C(1×1) surfaces and an asymmetric eight-layer slab containing both. Each of the calculations has been performed self-consistently in the scalar-relativistic limit, in which all relativistic effects except spin-orbit coupling are included.¹²

There are several reasons for carrying out calculations on the asymmetric slab as well as the two symmetric

slabs. First, comparison of the three sets of results provides an important consistency check. Second, the invariance of the work function and surface-state positions for a given surface between the appropriate pair of calculations has allowed us to verify that interactions between the surfaces are not significant. Because of computational limitations, this could not be verified by considering a substantially thicker slab. Finally, the asymmetric slab has the bulk stoichiometry, W_4C_4 , and this enables us to check possible Fermi level shifts in the W_5C_4 and W_4C_5 symmetric slabs. Such a test has not been demonstrated previously.

In the LAPW method,⁷ the unit cell is subdivided into muffin-tin (MT) spheres and an interstitial region. In addition, the slab geometry includes two surface regions. The LAPW wave function is continuous across each boundary and has a different analytic form in each region.¹³ Both the charge density and crystal potential are expressed in completely general form so that they are free from any shape approximations.¹⁴

The same MT radii, $R(W) = 1.20 \text{ \AA}$ and $R(C) = 0.96 \text{ \AA}$, have been assumed in both the bulk and slab calculations. These radii yield nearly-touching spheres along the nearest-neighbor W-C bond directions and provide similar convergence for both the W $5d$ and C $2p$ states. The calculations utilize a frozen-core approximation in which atomic charge densities are used to represent the W($\dots 4f^{14}5s^25p^6$) and C($1s^2$) core. Tails of the core charges outside the MT spheres are treated exactly. Exchange and correlation effects are treated in the local-density approximation using the Wigner interpolation formula.¹⁵

The bulk and slab wave functions are expressed as superpositions of LAPW's, with the expansion coefficients determined variationally. The bulk and slab calculations have included about 30 and 40 LAPW's per atom, respectively. This is expected to yield results which are converged to about 0.1 eV.

In the course of the self-consistency iterations, the LAPW valence charge density has been evaluated by using twelve special points¹⁶ to average over the bulk BZ.

Five special points were included in the slab calculations. Previous experience on analogous systems indicates that this sampling is sufficient to yield results which are converged within the overall 0.1-eV goal. The bulk calculation converged to a self-consistent solution within six iterations while the slab calculations required about twice as many cycles. In all cases, the final self-consistent eigenvalues were stable to better than 0.01 eV.

III. RESULTS AND DISCUSSION

A. Bulk electronic structure

The bulk energy-band results for hexagonal WC are shown in Fig. 2. Here, $E_n(\vec{k})$ is plotted along symmetry lines of the hexagonal Brillouin zone that is shown in Fig. 1. The symmetry of individual bands is indicated at the plot boundaries. The labels (s, p) at the interior symmetry points identify the principal angular momentum component of the LAPW wave function for each band. These correspond to the integral over the appropriate MT sphere of the s, p, d, \dots components of the LAPW charge density. The bands labeled s (p) have predominant C $2s$ ($2p$) weight. The unlabeled states have predominant W $5d$ character.

In addition to a low-lying C $2s$ band, the valence-band results feature a broad (~ 15 eV) eight-band $2p$ - $5d$ manifold which is approximately centered about the dashed Fermi energy E_F . The strong $2p$ - $5d$ admixture is such that approximately half the bands at or below E_F have predominant $2p$ and $5d$ character, respectively. This implies a nearly equal distribution of valence-band charge or a net charge transfer from W to C. This is expected from the corresponding electronegativities¹⁷ for W (1.7) and C (2.5). It is also consistent with the observed^{5,18} chemical shifts in the core levels of WC relative to elemental W and C.

A striking difference between the electronic properties of hexagonal WC and those of the cubic carbides is reflected in the density-of-states (DOS) curves. The DOS curve for WC is shown in Fig. 3. This curve has been cal-

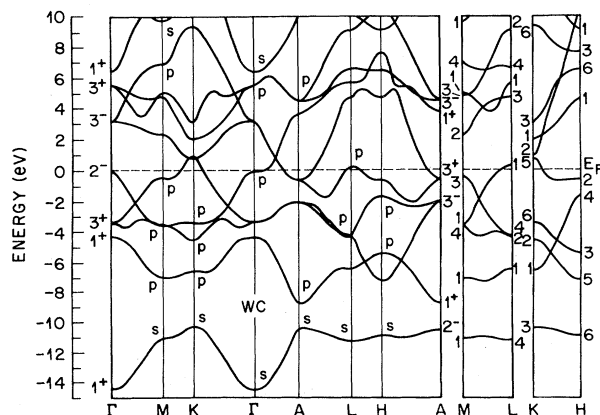


FIG. 2. LAPW $E(\vec{k})$ curves for bulk hexagonal WC. States labeled s or p have predominant C $2s$ - $2p$ weight in the C muffin-tin sphere; unlabeled states have predominant W $5d$ character.

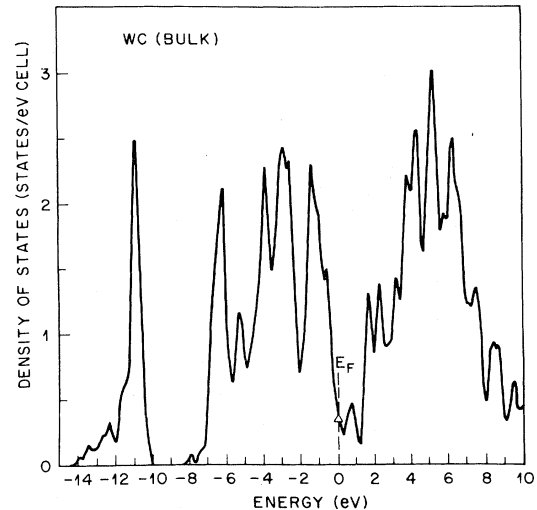


FIG. 3. Density-of-state curve for bulk WC. An experimental value, derived from heat-capacity measurements (Ref. 1), is shown by the triangle.

culated by a root-sampling procedure involving LAPW results at 70 special points. The individual levels were then broadened with a Gaussian function having a full width at half maximum (FWHM) of 0.3 eV. According to Fig. 3, the WC valence-band DOS curve for the eight-band $2p$ - $5d$ manifold is separated symmetrically into bonding and antibonding peaks which are joined by a DOS minimum near E_F . This contrasts with the cubic carbides,¹⁹ where the bonding-antibonding distribution is found to preserve the 3:5 ratio of the $2p$: $5d$ degeneracy.

The separation between the centers of gravity of the bonding and antibonding complexes is approximately 9 eV. This large "average gap" reflects a substantial covalent contribution to bonding in WC, which is certainly related to its hardness and high melting temperature. For comparison, the average gap in diamond is 13.5 eV.²⁰ If we correct for the ionic contribution to the WC gap based on Phillips's values for semiconductors with comparable electronegativity differences,²⁰ we find a purely covalent gap of about 7 eV.

The triangle at E_F in Fig. 3 represents the DOS value which is derived from heat-capacity measurements.¹ Although this experimental DOS value is renormalized by the factor $1+\lambda$ as a result of electron-phonon coupling, these corrections are expected to be small in WC, where superconductivity has not been observed²¹ at temperatures as low as 0.3 K.

Additional information regarding the shape and width of the occupied WC DOS is available from XPS measurements.^{5,18} The high-resolution valence-band spectrum of Colton *et al.*¹⁸ exhibits peaks at binding energies of 1.6, 3.2, and 7.0 eV. These are in good agreement with the calculated peaks at 1.5, 2.9–3.9, and 6.3 eV. According to soft-x-ray appearance potential spectroscopy (SXAPS) data,²² the unoccupied WC bands have an estimated width of 6.7 eV. This is also in good agreement with the calculated value of 7–8 eV.

The energy-band results of Fig. 2 characterize WC as a semimetal with a Fermi surface consisting of small pockets of electrons and holes. In particular, the calculations predict a single electron sheet centered at A plus several hole pockets at the L and K points and along the ΓA line. The calculated Fermi-surface dimensions are similar to those inferred from the de Haas-van Alphen data of Ishizawa and Tanaka.³ A detailed analysis of calculated and measured WC Fermi-surface properties will be deferred to a future publication.

B. Surface electronic structure

The present LAPW energy-band results for symmetric nine-layer WC(0001) slabs with exposed $W(1 \times 1)$ and $C(1 \times 1)$ faces are contained in Figs. 4(a) and 4(b), respectively. Using E_F as a common reference energy, $E(\vec{k}_{\parallel})$ is plotted along symmetry lines of the SBZ. As mentioned above, the $\Gamma\bar{M}\bar{K}$ triangle of the SBZ is identical in size and symmetry with the ΓMK wedge of the bulk BZ shown in Fig. 1. Although the number of valence electrons per primitive cell differs for the two slabs (46 versus 44), the overall results are relatively insensitive to the use of E_F as a reference energy. This is confirmed by a comparison of the LAPW results for an asymmetric eight-layer WC(0001) slab with those in Fig. 4, including surface-state and DOS features.

Those slab energy-band states that are connected by the solid lines in Figs. 4(a) and 4(b) represent surface states or surface resonances. These correspond to LAPW slab states whose MT weight is concentrated predominantly on the surface layers. The criteria for identifying these de-

pend on the distribution of the LAPW charge density within each of the MT spheres in the slab unit cell. The relevant quantity is the integral over the α th MT sphere of the square of the LAPW wave function, f_{α} . Since the wave function is normalized over all space (MT, surface, and interstitial regions), the sum over these MT contributions, $f \equiv \sum f_{\alpha} < 1$.

Those slab levels that are identified as surface states or surface resonances in Fig. 4 are such that (i) the surface-atom MT weight $f_S \geq 0.3f$, or (ii) the MT weight of the two outermost layers $f_S + f_{S-1} \geq 0.4f$. In either case, taking sums and differences of the appropriate surface-state pairs yields wave functions that are localized on either surface with a fractional MT weight of at least 0.6 on the outermost layer or 0.8 on the outermost pair.

The results in Fig. 4 exhibit an accumulation of surface-state bands within an energy range $E_F \pm 2$ eV for both the $W(1 \times 1)$ and $C(1 \times 1)$ surfaces. The only surface feature at lower energies occurs on the $C(1 \times 1)$ face. It corresponds to a C $2s$ surface-state band which is well localized on the surface for wave vectors \vec{k}_{\parallel} near the boundaries of the SBZ, where its binding energy is about 1.5 eV less than that for the bulk $2s$ band. This band becomes increasingly delocalized as \vec{k}_{\parallel} approaches $\bar{\Gamma}$, where it acquires a splitting (resulting from the finite thickness of the slab) of about 0.8 eV.

The surface-state bands that are derived from the symmetric nine-layer slab results of Fig. 4 are replotted to the right in Fig. 5. The results shown here satisfy the above criteria regarding LAPW MT weights as well as the symmetry requirement that surface states occur as appropriate

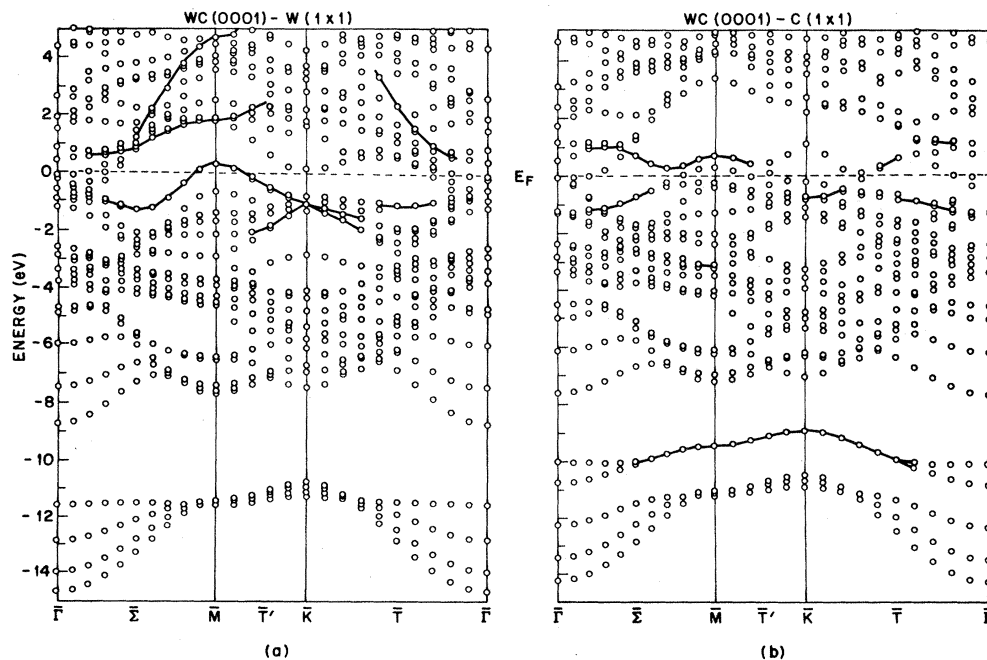


FIG. 4. LAPW energy-band results for symmetric nine-layer WC(0001) films with exposed $W(1 \times 1)$ and $C(1 \times 1)$ faces. Surface-state bands are indicated by the solid curves.

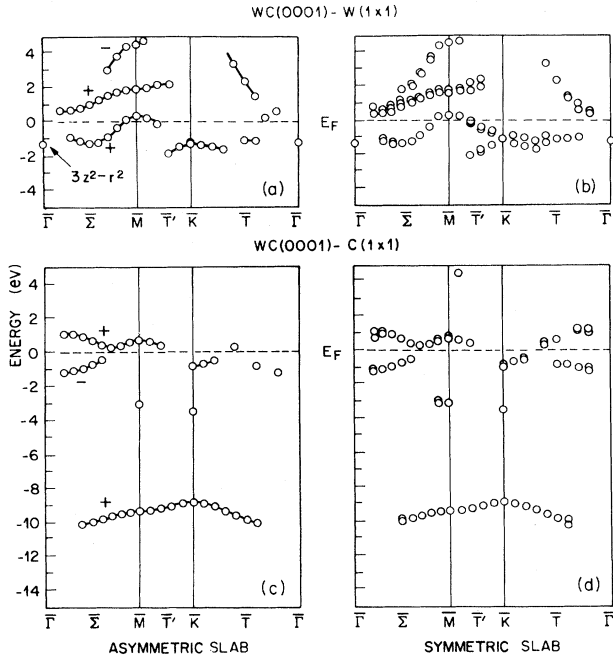


FIG. 5. Comparison of surface-state dispersion curves $E(\vec{k}_{\parallel})$ for $W(1 \times 1)$ and $C(1 \times 1)$ faces as determined from LAPW calculations on symmetric and asymmetric $WC(0001)$ slabs.

pairs of slab states. The finite splitting of the surface-state-band pairs, most evident near points at which they terminate and merge with the bulk band structure, vanishes in the thick-slab limit.

The results shown to the left in Fig. 5 have been obtained from LAPW calculations on an asymmetric eight-layer $WC(0001)$ thin film which contains both $W(1 \times 1)$ and $C(1 \times 1)$ faces. Since this slab no longer has a central reflection plane, the surface states no longer occur in pairs. The corresponding surface-state criteria for this asymmetric geometry are $f_S \geq 0.6f$ and $f_S + f_{S-1} \geq 0.8f$, respectively.

As shown in Fig. 5, the surface-state bands which are derived from the asymmetric and symmetric slab calculations are in generally good agreement. The two sets of results differ principally in regard to details such as the termination points of some surface-state bands. These minor differences are due to a combination of effects, including the finite thickness of the slabs, their 12% difference in thickness, and the rigid nature of the cutoff criteria for identifying surface states.

The symmetry and connectivity of the surface-state bands is indicated for the asymmetric slab results shown to the left in Fig. 5. The Σ line contains a vertical reflection plane so that the corresponding surface-state wave functions possess either even or odd reflection symmetry which is indicated. This symmetry is absent along both the \bar{T} and \bar{T}' lines, where the surface-state wave functions contain both even and odd components.

A single surface state is predicted at $\bar{\Gamma}$ for the $W(1 \times 1)$ surface. It has predominantly $(3z^2 - r^2)$ -type symmetry and a binding energy of about 1.2 eV. It disappears rap-

idly for $\vec{k}_{\parallel} \neq \vec{0}$. Although no detailed photoemission data have been reported thus far for $WC(0001)$, it is interesting to note that an analogous surface state has been observed at $\bar{\Gamma}$ in photoemission studies²³⁻²⁶ on $TiC(111)$ - $Ti(1 \times 1)$, where the surface geometry is similar. In particular, surface features have been observed at $\bar{\Gamma}$ with binding energies of 0.2 and 0.8 eV in these studies.

A tight-binding calculation²⁷ of the $TiC(111)$ surface-state properties has been carried out using a slab geometry and bulk band-structure parameters. This calculation predicts a single surface state at $\bar{\Gamma}$ for a $Ti(1 \times 1)$ surface with an energy that is above E_F by about 1 eV. Overall, these tight-binding results exhibit general features that are in qualitative agreement with the LAPW results of Fig. 5. This is particularly true if E_F is raised by 1–2 eV in the TiC results to accommodate, in rigid-band fashion, the extra two valence electrons of the WC molecular complex.

The concentration of surface-state bands within $E_F \pm 2$ eV for both the $W(1 \times 1)$ and $C(1 \times 1)$ faces of $WC(0001)$ is also reflected in the layer-projected DOS curves that are shown in Fig. 6. These curves have been calculated from the LAPW states at 14 special points in the irreducible triangle of the SBZ for symmetric nine-layer and asymmetric eight-layer slabs. The individual levels were then smoothed using a Gaussian function with a FWHM of 0.3 eV.

In each of the four panels, the separate curves represent the total slab DOS as well as the layer-projected DOS curves for a surface layer (S), first interior layer ($S-1$), etc. These layer-projected curves are calculated by weighting the total DOS by f_{α} , the LAPW weight in the

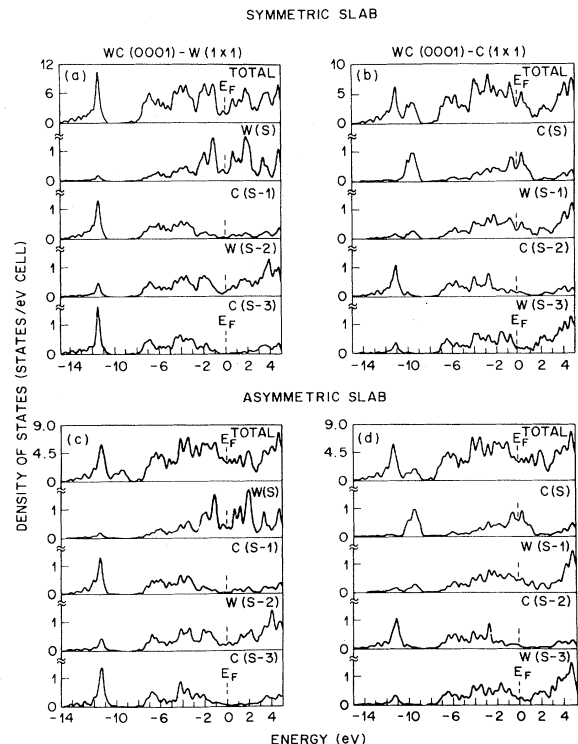


FIG. 6. Total and layer-projected density-of-state curves for $W(1 \times 1)$ and $C(1 \times 1)$ faces.

$\alpha=S, S-1, \dots$ MT spheres. The close similarity between the projected-DOS curves that are derived from the LAPW symmetric and asymmetric slab results is evident, both for the $W(1 \times 1)$ and $C(1 \times 1)$ surfaces.

For both faces, the surface-layer DOS near E_F is enhanced over that of the bulk while that of the first interior layer is affected to a lesser degree. Over an energy range $E_F \pm 2$ eV, the overall DOS enhancement relative to the bulk is larger for the $W(1 \times 1)$ surface. As expected from the $C(1 \times 1)$ surface-state dispersion curves of Figs. 4 and 5, a predominant feature of the $C(1 \times 1)$ surface DOS is a $2s$ peak at a 9.5-eV binding energy that is about 1.5 eV above that of the bulk $2s$ band.

As mentioned above, the calculated work function for the $W(1 \times 1)$ surface, $\phi(W)=5.2$ eV, is about 1.2 eV lower than that for the corresponding $C(1 \times 1)$ face, where $\phi(C)=6.4$ eV. (It is noted that the corresponding values derived from the symmetrical and asymmetrical slab calculations agree to within 0.03 eV.) This 1.2-eV difference in work functions implies, along with the corresponding electronegativities¹⁷ for W (1.7) and C (2.5), a net transfer of charge from W to C in the case of a $WC(0001)$ - $C(1 \times 1)$ surface. The work function $\phi(W)=5.2$ eV for the $W(1 \times 1)$ surface is close to the value ($\phi=5.25$ eV) observed²⁸ for $W\{110\}$, which has a similar density of surface atoms, namely, 0.14 \AA^{-2} .

The difference between the $C(1 \times 1)$ and $W(1 \times 1)$ work functions causes the charge density in the vacuum region above the $C(1 \times 1)$ surface to fall off more rapidly than

that for a $W(1 \times 1)$ face. This is illustrated in the right-hand portion of Fig. 7 where valence charge-density contours are plotted in a $(2\bar{1}\bar{1}0)$ plane containing the $[0001]$ and $[10\bar{1}0]$ axes. This plane is centered on one pair of nearest-neighbor W—C bond directions and also includes second-neighbor W or C atoms at a distance $\sqrt{3}a$ along $[10\bar{1}0]$. In the surface region where $\rho < 0.01$ electrons a.u.³, the neighboring contours differ by a factor of $\sqrt{10}$. Comparing the results for the $C(1 \times 1)$ and $W(1 \times 1)$ surfaces, it is seen that at a height c above a $C(1 \times 1)$ face, the charge density is an order of magnitude smaller than that above a $W(1 \times 1)$ surface. The corrugation amplitude is also more pronounced for the C surface; this suggests that He atom diffraction studies²⁹ may provide a valuable tool for identifying³⁰ the surface-layer composition of $WC(0001)$ samples.

The results shown on the left in Fig. 7 corresponds to valence charge densities for bulk WC. The plot origins have been chosen to facilitate a direct comparison between the bulk and slab results. In the bulk regions of each plot where $\rho > 0.01$ electrons a.u.³, the contour interval $\Delta\rho=0.01$. It is interesting to note that the charge contours just below the $W(1 \times 1)$ surface heal rapidly to their bulk form within an atomic radius of the surface. This healing is more gradual near the $C(1 \times 1)$ surface. Here, the nearest-neighbor C—W bond charge density is enhanced and the charge contours surrounding the W atoms at the underlayer sites are noticeably deformed in comparison with those for the bulk.

While the present study of the surface electronic structure of WC has been restricted to (0001) -type surfaces, it is worthwhile to consider briefly the implications of these results in regard to the catalytic properties⁴ of WC. The surface-state bands near E_F in Fig. 5 for the $W(1 \times 1)$ and $C(1 \times 1)$ faces represent “dangling-bond”-type states which are caused by the truncation of bonds at the surface. One expects analogous surface-state bands to occur on other crystal faces, through their multiplicity will depend undoubtedly on the number of broken nearest-neighbor W—C bonds. The resulting enhancement of the surface DOS for powder samples with a variety of exposed faces should provide a favorable environment for catalytic processes.

A recent study of catalytic properties of WC by Ross and Stonehart³¹ illustrates the complexity of the problem. They have shown that the ability of WC to exhibit Pt-like behavior in regard to hydrogen chemisorption is extremely sample and treatment dependent. In particular, they find that the “active” material has a surface composition which is different from the bulk and consistently C deficient. They identify the excess W with an increase in the active sites available for hydrogen chemisorption. However, as Bennett *et al.*³² have pointed out, it is possible to have excess W on the surface without any deviation from stoichiometry simply by exposing the appropriate crystal faces. Thus, the difference between WC powders showing high and low hydrogen chemisorption may be due to the preferential exposure of optimum crystallite faces depending on the method of preparation. Clearly, single-crystal surface studies will be helpful in resolving this and other issues regarding the catalytic properties of WC.

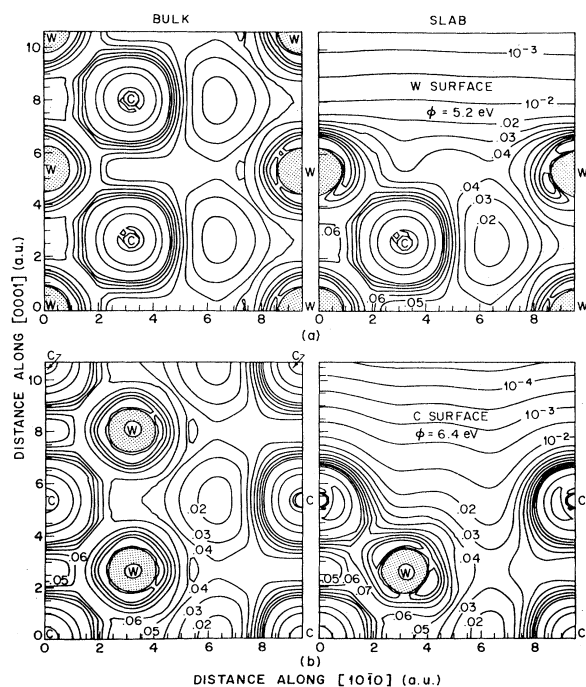


FIG. 7. Comparison of bulk and slab LAPW valence charge-density results in a $(2\bar{1}\bar{1}0)$ plane. Adjacent bulk contours differ by 0.01 electrons/a.u.³, while those in the vacuum region ($\rho < 0.01$) scale by the factor $\sqrt{10}$.

IV. CONCLUSIONS

The present LAPW results for hexagonal WC suggest that the strength and stability of this compound is due primarily to the formation of strong nearest-neighbor W—C bonds. This is reflected both in the valence-electron charge-density plots in Fig. 7 and, less directly, in the valence-band DOS curve in Fig. 3. According to Fig. 3, the WC valence-band DOS exhibits a minimum near the middle of the eight-band C $2p$ —W $5d$ bonding-antibonding manifold. This is in sharp contrast to the corresponding DOS curves for the group-IVB and -VIB carbides,¹⁹ which crystallize with the rocksalt structure. The rocksalt-structure DOS minimum occurs near E_F for the group-IVB compounds so that in terms of a simple rigid-band picture, the structure becomes increasingly destabilized as the extra electrons of the group-VB and -VIB elements begin filling the higher-energy antibonding subbands. This destabilization effect is partially compensated by a lowering of the d bands relative to the C $2p$ states,¹⁹ but apparently this is insufficient for stabilizing the group-VIB compounds.

The bulk WC DOS is in satisfactory agreement with XPS (Refs. 5 and 18) and SXAPS (Ref. 22) data in regard to the overall $2p$ - $5d$ bandwidth (~ 15 eV) and the similar widths (~ 7 – 8 eV) of the occupied and unoccupied portions. The WC Fermi surface is that of a semimetal, consisting of several small electron and hole sheets. The calculated dimensions are qualitatively consistent with those

inferred from de Haas—van Alphen data,³ though a quantitative comparison has not yet been carried out. Qualitatively, the angular dependence of various branches of the de Haas—van Alphen data exhibit features characteristic of the electron sheet at A and the hole pockets at K and along ΓA . However, these data do not appear to contain any indication of hole pockets at L that are predicted by the LAPW results in Fig. 2. A more detailed analysis will be required in order to clarify the relationship between the calculated and observed WC Fermi surface.

A critical evaluation of the calculated WC(0001) surface-state features must await future experimental studies on the surface properties of this material. A distinctive feature of these results is the accumulation of surface-state bands near E_F for both the W(1 \times 1) and C(1 \times 1) faces. This produces an enhanced surface-layer density of states near E_F , a factor which could be important for understanding the catalytic properties of WC.

ACKNOWLEDGMENTS

We are pleased to acknowledge useful discussions with our colleagues S. D. Kevan, J. C. Phillips, and N. V. Smith on various aspects of this investigation. We are particularly grateful to Dr. Hiromoto Uwe for providing an excellent translation of Ref. 3.

- ¹L. E. Toth, *Transition Metal Carbides and Nitrides* (Academic, New York, 1971).
- ²K. Bachmann and W. S. Williams, *J. Appl. Phys.* **42**, 4406 (1971).
- ³Y. Ishizawa and T. Tanaka, *Solid State Phys. (Japan)* **16**, 41 (1981).
- ⁴R. B. Levy and M. Boudart, *Science* **181**, 547 (1973).
- ⁵L. H. Bennett, J. R. Cuthill, A. J. McAlister, N. E. Erickson, and R. E. Watson, *Science* **184**, 563 (1974).
- ⁶T. H. Geballe, *Rev. Mod. Phys.* **36**, 134 (1964).
- ⁷O. K. Andersen, *Phys. Rev. B* **12**, 3060 (1975).
- ⁸F. Herman, R. V. Kasowski, P. M. Stefan, and W. E. Spicer, *Bull. Am. Phys. Soc.* **27**, 249 (1982).
- ⁹E. S. Alekseev, R. G. Arkhipov, and S. V. Popova, *Phys. Status. Solidi B* **110**, K151 (1982).
- ¹⁰M. Lax, *Symmetry Principles in Solid State and Molecular Physics* (Wiley, New York, 1974).
- ¹¹A. W. Luehrmann, *Adv. Phys.* **17**, 1 (1968).
- ¹²D. R. Hamann, L. F. Mattheiss, and H. S. Greenside, *Phys. Rev. B* **24**, 6151 (1981).
- ¹³O. Jepsen, J. Madsen, and O. K. Andersen, *Phys. Rev. B* **18**, 605 (1978).
- ¹⁴E. Wimmer, H. Krakauer, M. Weinert, and A. J. Freeman, *Phys. Rev. B* **24**, 864 (1981).
- ¹⁵E. Wigner, *Phys. Rev.* **46**, 1002 (1934).
- ¹⁶H. J. Monkhorst and J. D. Pack, *Phys. Rev. B* **13**, 5188 (1976).
- ¹⁷L. Pauling, *The Nature of the Chemical Bond*, 3rd ed. (Cornell University Press, Ithaca, New York, 1960).
- ¹⁸R. J. Colton, J.-T. L. Huang, and J. W. Rabalais, *Chem. Phys. Lett.* **34**, 337 (1975); R. J. Colton and J. W. Rabalais, *Inorg. Chem.* **15**, 236 (1976).
- ¹⁹B. M. Klein, D. A. Papaconstantopoulos, and L. L. Boyer, *Phys. Rev. B* **22**, 1946 (1980).
- ²⁰J. C. Phillips, *Bonds and Bands in Semiconductors* (Academic, New York, 1973), p. 42.
- ²¹R. H. Willens and E. Buehler, *Appl. Phys. Lett.* **7**, 25 (1965).
- ²²J. E. Houston, G. E. Laramore, and R. L. Park, *Science* **185**, 258 (1974).
- ²³A. M. Bradshaw, J. F. van der Veen, F. J. Himpsel, and D. E. Eastman, *Solid State Commun.* **37**, 37 (1980).
- ²⁴J. H. Weaver, A. M. Bradshaw, J. F. van der Veen, F. J. Himpsel, D. E. Eastman, and C. Politis, *Phys. Rev. B* **22**, 4921 (1980).
- ²⁵C. Oshima, M. Aono, S. Zaima, Y. Shibata, and S. Kawai, *J. Less-Common Metals* **82**, 69 (1981).
- ²⁶A. Callenas, L. I. Johansson, A. N. Christensen, K. Schwarz, and J. Redinger, *Phys. Rev. B* **27**, 5934 (1983).
- ²⁷A. Fujimori, F. Minami, and N. Tsuda, *Surf. Sci.* **121**, 199 (1982).
- ²⁸T. V. Vorburger, D. Penn, and E. W. Plummer, *Surf. Sci.* **48**, 417 (1975).
- ²⁹M. J. Cardillo, G. E. Becker, D. R. Hamann, J. A. Serri, L. Whitman, and L. F. Mattheiss, *Phys. Rev. B* **28**, 494 (1983).
- ³⁰D. R. Hamann, *Phys. Rev. Lett.* **46**, 1227 (1981).
- ³¹P. N. Ross, Jr. and P. Stonehart, *J. Catalysis* **39**, 298 (1975).
- ³²L. H. Bennett, A. J. McAlister, J. R. Cuthill, N. E. Erickson, and R. E. Watson, *J. Mol. Catalysis* **2**, 203 (1977).